Metals **2014**, *4*, 597-608; doi:10.3390/met4040597

OPEN ACCESS

metals

ISSN 2075-4701

www.mdpi.com/journal/metals/

Article

Corrosion and Serration Behaviors of $TiZr_{0.5}NbCr_{0.5}V_xMo_y$ High Entropy Alloys in Aqueous Environments

Jiemin Li [1], Xiao Yang [1,2], Ruanli Zhu [3] and Yong Zhang [1,*]

[1] State Key Laboratory for Advanced Metals and Materials, University of Science and Technology Beijing, Xueyuan Road 30#, Beijing 100083, China; E-Mail: lijiemin_01@163.com

[2] State Key Laboratory for Advanced Metallurgy, University of Science and Technology Beijing, Xueyuan Road 30#, Beijing 100083, China; E-Mail: yangxiao_sky@163.com

[3] Institute for Advanced Materials and Technology, University of Science and Technology Beijing, Xueyuan Road 30#, Beijing 100083, China; E-Mail: zhuruanli@163.com

* Author to whom correspondence should be addressed; E-Mail: drzhangy@ustb.edu.cn; Tel.: +86-10-6233-3073.

External Editor: Hugo Lopez

Received: 4 November 2014; in revised form: 2 December 2014 / Accepted: 11 December 2014 / Published: 15 December 2014

Abstract: The corrosion and serration behaviors of $TiZr_{0.5}NbCr_{0.5}$, $TiZr_{0.5}NbCr_{0.5}V$ and $TiZr_{0.5}NbCr_{0.5}Mo$ high entropy alloys (HEAs) in NaCl and H_2SO_4 solutions were studied by potentiodynamic polarizations (PP) and immersion tests. The results show that all the alloys display excellent corrosion resistance no matter in NaCl solution or in H_2SO_4 solution. The additions of V and Mo increase the pitting corrosion resistance for the three alloys in NaCl solution slightly and greatly improve the corrosion resistance in H_2SO_4 solution. The corrosion behaviors of $TiZr_{0.5}NbCr_{0.5}$ and $TiZr_{0.5}NbCr_{0.5}Mo$ alloys are more sensitive to temperature than that of $TiZr_{0.5}NbCr_{0.5}V$ alloy. After immersion, the surface of $TiZr_{0.5}NbCr_{0.5}$ alloy appears some pitting holes, this may be related to the electrochemical noise and serration behavior on PP curves; localized corrosion initiates mainly on the boundaries of the BCC and Cr_2Zr Laves phase for $TiZr_{0.5}NbCr_{0.5}V$ alloy; while for the $TiZr_{0.5}NbCr_{0.5}Mo$ alloy, the dendrites with Mo element rich region exhibit poor corrosion resistance.

Keywords: high-entropy alloy; potentiodynamic polarization; immersion test; electrochemical noise; serration behavior

1. Introduction

High-entropy alloys (HEAs), which may be defined as alloys that generally contain more than three principal elements and each of them has an atomic percentage more than 5 at.% [1–7], have attracted increasing attentions due to their extensive applications prospect. Because of the very high mixing entropy, HEAs usually intend to form face center cubic (FCC) and/or body center cubic (BCC) disordered solid solutions (DSS) rather than intermetallic compounds or other complex ordered phases [8]. The particular structure makes multi-component HEAs exhibit excellent properties, such as high strength [7], high ductility [9,10], well magnetic properties [11], excellent resistances to wear, oxidation, irradiation and corrosion [5,12,13], and high thermal stability [14]. These properties provide HEAs with many potential applications such as tools, molds, diffusion barriers for integrated circuit (IC) and solar thermal collectors, *etc*., and a number of HEAs have been developed for both functional and structural applications.

Recently, the HEAs with promising high-temperature mechanical properties are designed by the phase formation rules of HEAs and based on some transition metal elements with high melting point such as Ta, Mo, Nb, W, V, and Ti. $Nb_{25}Mo_{25}Ta_{25}W_{25}$ and $V_{20}Nb_{20}Mo_{20}Ta_{20}W_{20}$ alloys have been proven to remain stable, still presenting a single-phase BCC crystal structure after exposure to 1400 °C, and exhibit a strong resistance to high-temperature softening, likely due to slow diffusion effects of atoms in multicomponent alloys [5]. $NbTiVTaAl_x$ alloys have a single DSS phase with BCC structure and possess high compressive yield strength and high ductility (no fracture under 50% strains) [15]. Senkov *et al.* found that $NbCrMo_{0.5}Ta_{0.5}TiZr$ alloy has a good combination of mechanical properties and oxidation resistance after heating at 1273 K for 100 h in flowing air [14].

In this paper, corrosion behaviors of the $TiZr_{0.5}NbCr_{0.5}V_xMo_y$ alloys in NaCl and H_2SO_4 solutions were studied by the measurements of PP curves, and electrochemical noise and serration behaviors were observed on the PP curves.

2. Results

2.1. Microstructure Analysis

Figure 1 shows the XRD patterns of $TiZr_{0.5}NbCr_{0.5}$, $TiZr_{0.5}NbCr_{0.5}V$ and $TiZr_{0.5}NbCr_{0.5}Mo$ refractory alloys. All the alloys exhibit the reflections of a BCC DSS phase and an ordered Cr_2Zr phase, indicating that the additions of V or Mo have little effect on the phase constitution of $TiZr_{0.5}NbCr_{0.5}$ alloy and only make the diffraction peaks shift to the right side. Taking into account that the intensities of the diffraction peaks of BCC DSS phase are frequently stronger than that of ordered phases, the volume fractions of DSS appear to dominate and can be considered as the major phase. As listed in Table 1, the values of mixing enthalpy($\Delta H_{\mathrm{mix}}^{AB}$)among all the constituent elements, we can see that Zr has the most negative mixing enthalpy with Cr, and this may be the reason why intermetallic compound phase Cr_2Zr forms.

Figure 2 shows the SEM secondary electron images of $TiZr_{0.5}NbCr_{0.5}$, $TiZr_{0.5}NbCr_{0.5}V$ and $TiZr_{0.5}NbCr_{0.5}Mo$ alloys. Clearly, typical cast dendritic and inter-dendritic morphologies can be observed in all the alloys, as marked by arrows in the figure (marks of "ID" for inter-dendrites, and "DR" for dendrites). The dendrites of $TiZr_{0.5}NbCr_{0.5}V$ and $TiZr_{0.5}NbCr_{0.5}Mo$ alloys are much smaller than that of $TiZr_{0.5}NbCr_{0.5}$ alloy, which indicates that the additions of V and Mo make the dendrites refined. V and Mo elements can also lead to a significant decrease in the grain size in the Fe based steels, mainly due to the increasing driving force for nucleation of the refractory particles of V(C,N) or other particles [14,15]. According to the EDS analysis listed in Table 2, the inter-dendrites of the three alloys are rich in Zr and Cr elements.

Figure 1. XRD patterns of the as-solidified $TiZr_{0.5}NbCr_{0.5}$, $TiZr_{0.5}NbCr_{0.5}V$ and $TiZr_{0.5}NbCr_{0.5}Mo$ alloys.

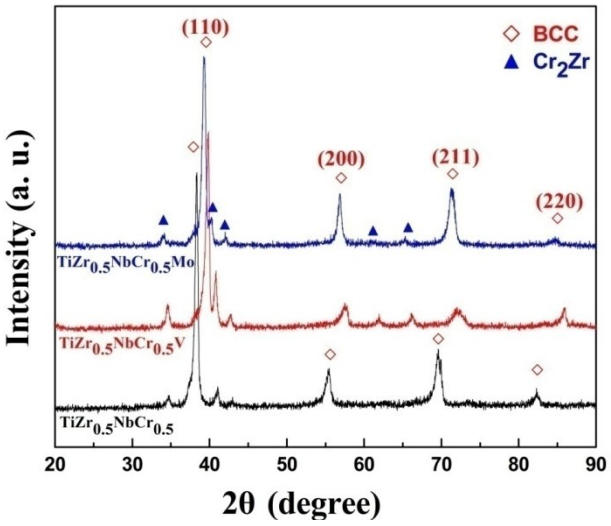

Figure 2. SEM secondary electron images of the (**a**) $TiZr_{0.5}NbCr_{0.5}$; (**b**) $TiZr_{0.5}NbCr_{0.5}V$; (**c**) $TiZr_{0.5}NbCr_{0.5}Mo$ alloys.

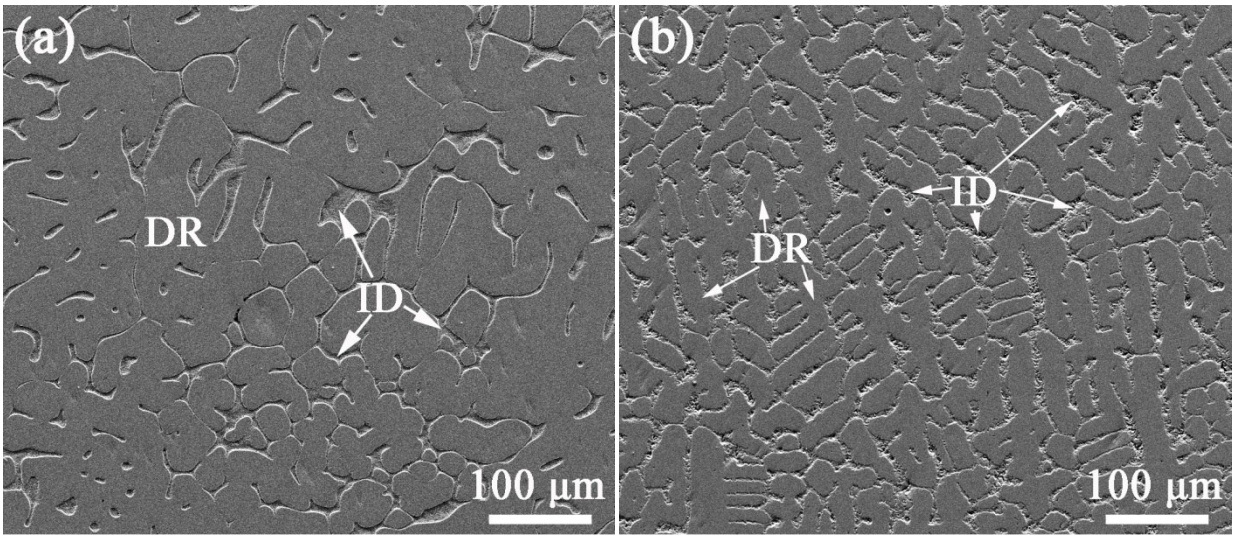

Figure 2. *Cont.*

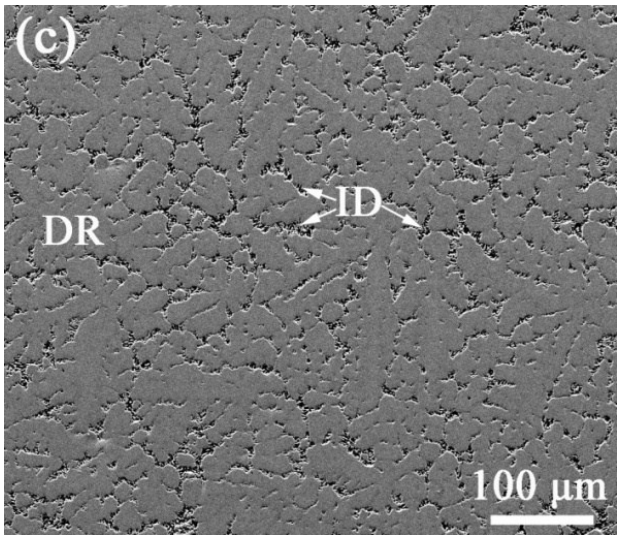

Table 1. Chemical mixing enthalpy ($\Delta H_{\mathrm{mix}}^{AB}$) of a pair of atoms.

Elements	Ti	Zr	Nb	Cr	V	Mo
Ti	0	0	2	−7	−2	−4
Zr		0	4	−12	−4	−6
Nb			0	−7	−1	−6
Cr				0	−2	0

Table 2. EDS analyses (at.%) for $TiZr_{0.5}NbCr_{0.5}$, $TiZr_{0.5}NbCr_{0.5}V$, $TiZr_{0.5}NbCr_{0.5}Mo$ alloys.

Alloys	Phases and states		Ti	Zr	Nb	Cr	V	Mo
$TiZr_{0.5}NbCr_{0.5}$		nominal	33.33	16.67	33.33	16.67		
	ID	Before immersed	27.13	27.32	14.07	31.48		
		After immersed	26.60	25.76	16.29	31.34		
	DR	Before immersed	32.25	14.53	41.11	12.11		
		After immersed	32.09	14.57	40.17	13.17		
$TiZr_{0.5}NbCr_{0.5}V$		nominal	25.00	12.50	25.00	12.50	25.00	
	ID	Before immersed	15.84	24.59	11.95	21.62	25.99	
		After immersed	14.93	23.26	14.23	22.47	25.11	
	DR	Before immersed	25.99	8.52	25.43	12.79	27.27	
		After immersed	25.48	8.34	28.61	10.88	26.69	
$TiZr_{0.5}NbCr_{0.5}Mo$		nominal	25.00	12.50	25.00	12.50		25.00
	ID	Before immersed	19.87	30.98	12.08	26.39		10.68
		After immersed	18.75	32.79	10.36	27.84		10.27
	DR	Before immersed	21.30	8.05	31.42	6.85		32.37
		After immersed	22.42	9.8	30.08	8.86		28.84

2.2. Corrosion Behaviors

2.2.1. Potentiodynamic Polarization (PP) Measurements

PP curves of $TiZr_{0.5}NbCr_{0.5}$, $TiZr_{0.5}NbCr_{0.5}V$ and $TiZr_{0.5}NbCr_{0.5}Mo$ alloys in 3.5 wt.% NaCl solution at room temperature are given in Figure 3a and the electrochemical parameters are listed in Table 3. All the alloys exhibit good resistance to general corrosion, and show low corrosion current density (i_{corr}) which are about 4.41×10^{-9}, 9.74×10^{9}, 9.40×10^{-8} A/cm^2, respectively. They all show excellent ability to passivation and exhibit a wide passive region (ΔE) extending >1400 mV in the sodium chloride solution. Generally, many alloys cannot develop passivation or have a narrow passive region in NaCl solution [3,16–19], this is due to chloridion (Cl^-) may penetrate and damage the passive film. The elements, Ti, Zr, Nb, Cr, Mo, and V, have strong passivation abilities which facilitate to form oxide films, and the films are with multicomponent high entropy alloys, with dense packing structure, and chloridion cannot easily penetrate through. This film resists the penetration of chloridion and improves their pitting potential which is associated with an increasing resistance to pitting.

Figure 3. Potentiodynamic polarization curves of $TiZr_{0.5}NbCr_{0.5}$, $TiZr_{0.5}NbCr_{0.5}V$ and $TiZr_{0.5}NbCr_{0.5}Mo$ alloys (**a**) in 3.5 wt.% NaCl solution (**b**) in 0.5 M H_2SO_4 solution.

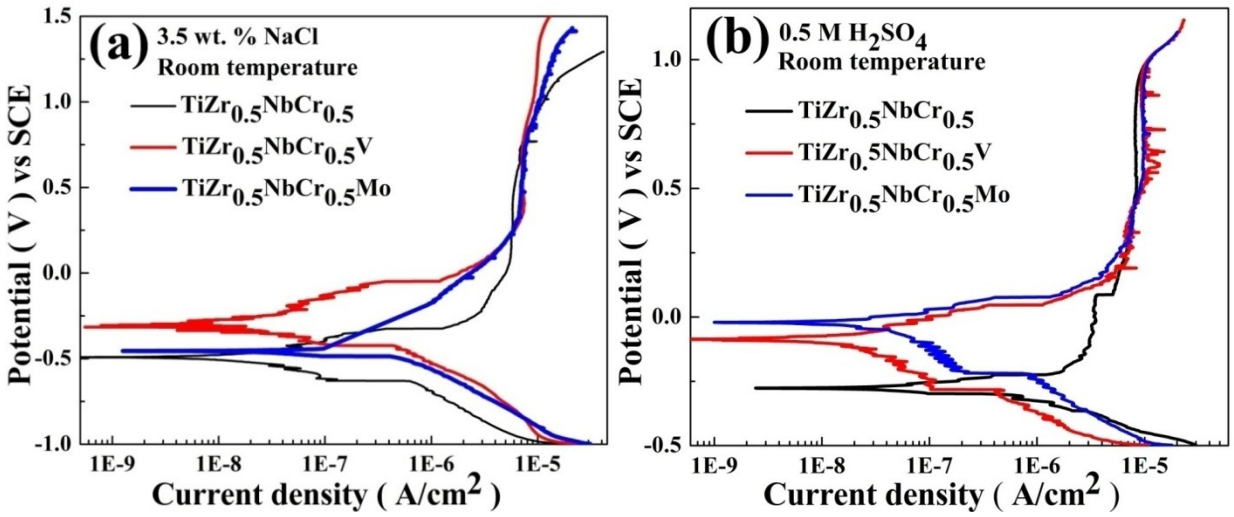

Figure 3b presents PP tests of $TiZr_{0.5}NbCr_{0.5}$, $TiZr_{0.5}NbCr_{0.5}V$ and $TiZr_{0.5}NbCr_{0.5}Mo$ alloys in 0.5 M H_2SO_4 solution at 25 °C. The electrochemical parameters are also listed in Table 3. In sulfuric acid solution, three alloys all show excellent resistance to the general corrosion, and their corrosion current density can reach to 4.52×10^{-7}, 2.04×10^{-8}, and 5.26×10^{-8} A/cm^2, respectively. Compared with $TiZr_{0.5}NbCr_{0.5}$ alloy, V and Mo elements make the corrosion potential (E_{corr}) shift positively and the corrosion current density decrease, which show that $TiZr_{0.5}NbCr_{0.5}V$ and $TiZr_{0.5}NbCr_{0.5}Mo$ alloys have better corrosion resistance than that of $TiZr_{0.5}NbCr_{0.5}$ alloy in the H_2SO_4 solution.

Table 3. Electrochemical parameters of $TiZr_{0.5}NbCr_{0.5}$, $TiZr_{0.5}NbCr_{0.5}V$ and $TiZr_{0.5}NbCr_{0.5}Mo$ alloys.

Alloys	Type of solutions	Temperature	E_{corr}(V_{SCE})	I_{corr}(μA/cm^2)	E_{pit}(V_{SCE})	ΔE(V)
$TiZr_{0.5}NbCr_{0.5}$	H_2SO_4	25 °C	−0.277	0.452	0.968	1.170
	NaCl	25 °C	−0.489	0.00441	1.180	1.480
		40 °C	−0.327	0.211	0.954	1.127
		55 °C	−0.372	0.522	0.783	0.994
$TiZr_{0.5}NbCr_{0.5}V$	H_2SO_4	25 °C	−0.087	0.02039	0.998	0.943
	NaCl	25 °C	−0.311	0.00974	1.448	1.482
		40 °C	−0.293	0.0247	1.115	1.344
		55 °C	−0.332	0.0765	1.097	1.260
$TiZr_{0.5}NbCr_{0.5}Mo$	H_2SO_4	25 °C	−0.018	0.0526	0.984	0.944
	NaCl	25 °C	−0.455	0.0940	1.400	1.820
		40 °C	−0.403	0.223	1.363	1.690
		55 °C	−0.345	0.458	1.224	1.482

The corrosion behaviors of $TiZr_{0.5}NbCr_{0.5}$, $TiZr_{0.5}NbCr_{0.5}V$ and $TiZr_{0.5}NbCr_{0.5}Mo$ alloys at 25 °C, 40 °C and 55 °C in NaCl solution are showed in Figure 4. From Figure 4a–c, a rising temperature increases the corrosion current density, the corrosion potential, and the current density of passivation, but decreases the pitting potential for $TiZr_{0.5}NbCr_{0.5}$, $TiZr_{0.5}NbCr_{0.5}V$ and $TiZr_{0.5}NbCr_{0.5}Mo$ alloys. For the three alloys, with temperature increasing, the corrosion rate which is directly related to i_{corr} increasing and the pitting corrosion is easier to happen. As the solution temperature increasing, the corrosion potential shifts positively, the critical passive current density increases. Thus, the resistance to corrosion decreases as the temperature increases. $TiZr_{0.5}NbCr_{0.5}V$ alloy is the least sensitive to temperature among the three alloys, indicating that the passive film generated on the surface of $TiZr_{0.5}NbCr_{0.5}V$ alloy is the most stable and insensitive to external environment. However, for the $TiZr_{0.5}NbCr_{0.5}$ and $TiZr_{0.5}NbCr_{0.5}Mo$ alloys, their electrochemical parameters change a lot with the increasing of temperature. More serrations can be seen on the PP curves at 40 °C and 55 °C than at room temperature for the three alloys, but the reason still remain unknown.

Figure 4. Polarization diagrams for (**a**) $TiZr_{0.5}NbCr_{0.5}$; (**b**) $TiZr_{0.5}NbCr_{0.5}V$; (**c**) $TiZr_{0.5}NbCr_{0.5}Mo$ alloys at various temperatures in 3.5 wt.% NaCl solution.

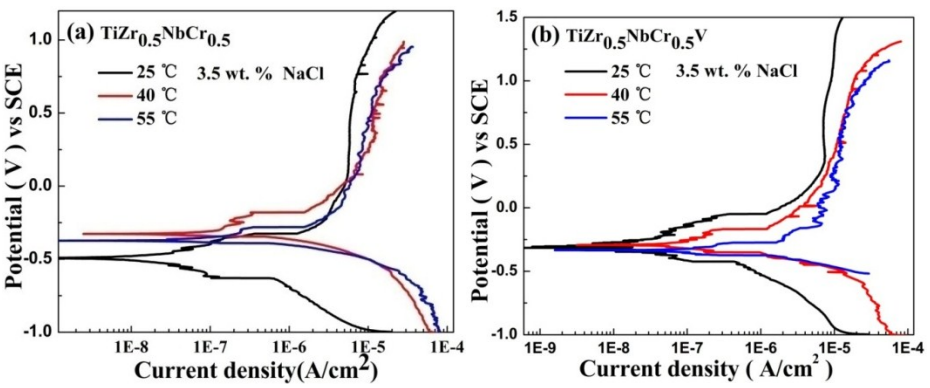

Figure 4. *Cont.*

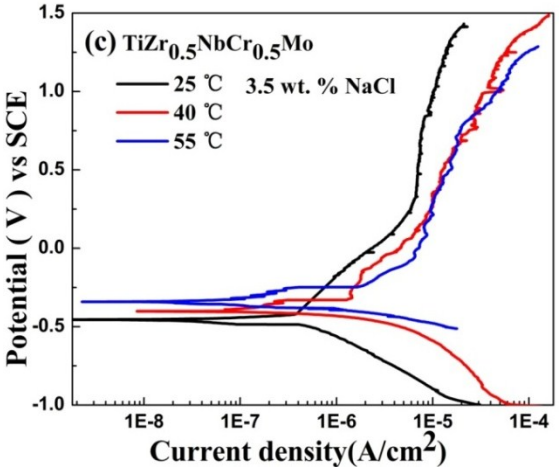

2.2.2. Immersion Tests

The surface morphology of $TiZr_{0.5}NbCr_{0.5}$, $TiZr_{0.5}NbCr_{0.5}V$ and $TiZr_{0.5}NbCr_{0.5}Mo$ alloys after immersed in 3.5 wt.% NaCl solution for 15 days are showed in Figure 5 and the EDS analyses are listed in Table 3. The major corrosion model of $TiZr_{0.5}NbCr_{0.5}$ alloy belongs to pitting, because some pitting holes are found, as shown by arrows. This indicates that $TiZr_{0.5}NbCr_{0.5}$ alloy has a poor resistance to pitting corrosion. For $TiZr_{0.5}NbCr_{0.5}V$ and $TiZr_{0.5}NbCr_{0.5}Mo$ alloys, some regions on the surface initiate mild localized corrosion. The regions in which the corrosion originates for $TiZr_{0.5}NbCr_{0.5}V$ alloy concentrate mainly on the boundaries of the BCC phase and Cr_2Zr phase, while the locations of corrosion for $TiZr_{0.5}NbCr_{0.5}Mo$ alloy are in the dendrites, as marked by the arrows. From the EDS analyses, there are no obvious difference between the samples before and after immersion for $TiZr_{0.5}NbCr_{0.5}$ and $TiZr_{0.5}NbCr_{0.5}V$ alloys. However, for the $TiZr_{0.5}NbCr_{0.5}Mo$ alloy, the content of Mo in the dendrites is decreased, indicating that Mo element in the dendrites is prone to corrosion. This result coincides with the surface appearances of $TiZr_{0.5}NbCr_{0.5}Mo$ alloy which easily produces the selective corrosion in the dendrites.

Figure 5. Surface morphology of alloys after immersion tests in 3.5 wt.% NaCl solution for 15 days: (**a**) $TiZr_{0.5}NbCr_{0.5}$; (**b**) $TiZr_{0.5}NbCr_{0.5}V$ and (**c**) $TiZr_{0.5}NbCr_{0.5}Mo$ alloys.

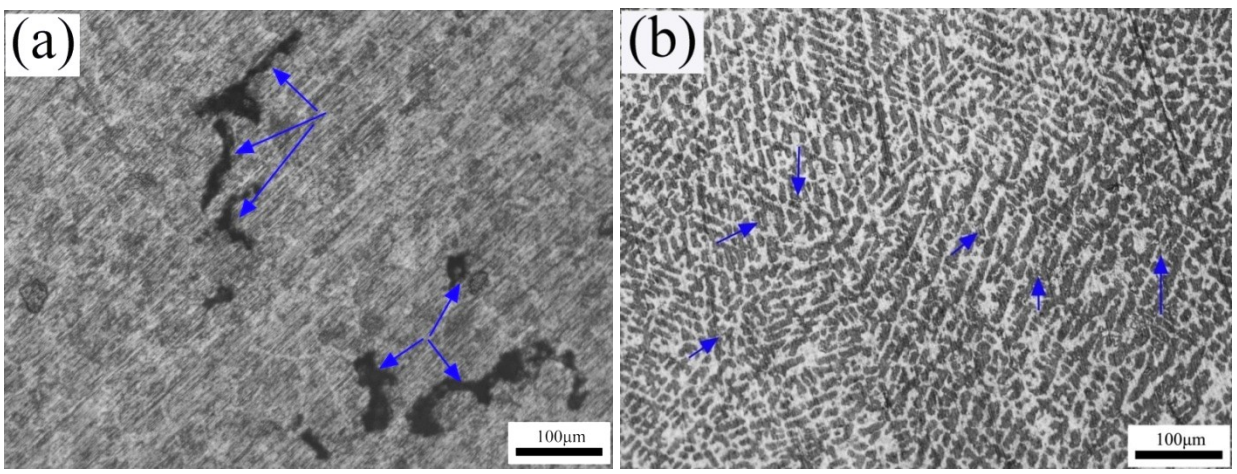

Figure 5. *Cont.*

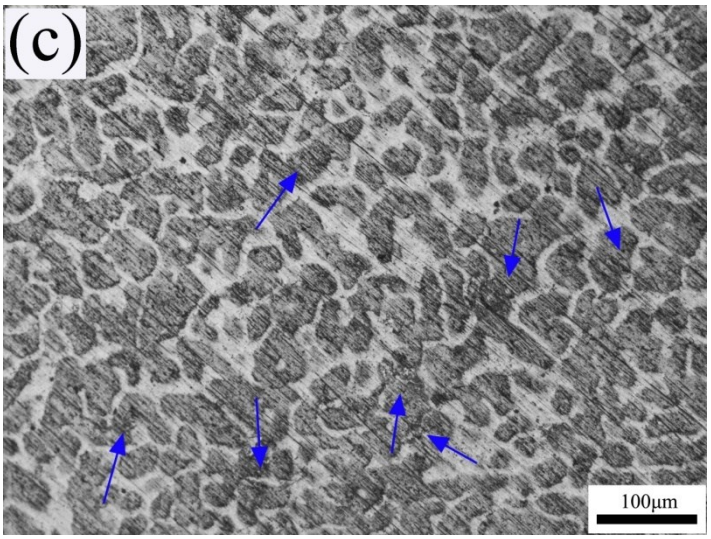

3. Discussion

If the surface examination shows the major types of corrosion are localized corrosion and/or pitting, the corrosion rate is usually determined using electrochemical-polarization measurements [20]. The corrosion rate r is expressed as:

$$r(\text{mm / year}) = 3.27 \times 10^{-3} \times \frac{i_{corr}}{\rho} \times EW \quad (1)$$

where ρ is the density of the alloy in g/cm^3, EW is the alloy equivalent weight, which is given by:

$$EW = \left(\sum \frac{n_i f_i}{W_i} \right)^{-1} \quad (2)$$

where n_i is the valence of the i_{th} element of the alloy, f_i is the atom fraction of the i_{th} element of the alloy, and W_i is the atomic weight of the i_{th} element of the alloy.

In this work, as listed in Table 3, $TiZr_{0.5}NbCr_{0.5}$ alloy has the minimum corrosion current density and the most active corrosion potential, and $TiZr_{0.5}NbCr_{0.5}Mo$ alloy has the maximum i_{corr} and medium E_{corr} in the NaCl solution at 25 °C among the three alloys. According to Equations (1) and (2), the corrosion rates of $TiZr_{0.5}NbCr_{0.5}$, $TiZr_{0.5}NbCr_{0.5}V$ and $TiZr_{0.5}NbCr_{0.5}Mo$ alloys are 3.46×10^{-5}, 6.85×10^{-5} and 6.60×10^{-4} mm/y, respectively. The result indicates that the resistance to general corrosion was slightly decreased after adding vanadium to the refractory $TiZr_{0.5}NbCr_{0.5}$ alloy, and molybdenum makes the anti-corrosion properties declined more significantly. The reason why the $TiZr_{0.5}NbCr_{0.5}V$ and $TiZr_{0.5}NbCr_{0.5}Mo$ alloys has larger corrosion rate than $TiZr_{0.5}NbCr_{0.5}$ alloy may be that V and Mo elements prompt the precipitation of Cr_2Zr phase and increase its dispersion which can make potential differences in small areas and induce the general corrosion. Furthermore, there is little difference in the passive current density (i_{pass}) for the $TiZr_{0.5}NbCr_{0.5}$, $TiZr_{0.5}NbCr_{0.5}V$ and $TiZr_{0.5}NbCr_{0.5}Mo$ alloys, which indicate the dissolution rates of the oxide films formed are very similar. The pitting potentials are 1.180, 1.448, and 1.400 V_{SCE} for $TiZr_{0.5}NbCr_{0.5}$, $TiZr_{0.5}NbCr_{0.5}V$ and $TiZr_{0.5}NbCr_{0.5}Mo$ alloys, respectively, and pitting holes are only found on the surface of $TiZr_{0.5}NbCr_{0.5}$ alloy. Molybdenum can improve the

ability of passivation in the non-oxidization medium and the resistance to pitting. General view is that the molybdenum atoms are adsorbed to the surface of the active metal in the form of MoO_4^{2-}, which inhibit the dissolution of active metal atoms and improve the pitting resistance. Like the Mo element, Vanadium also can form a dense passive film and make the ability of the resistance to pitting corrosion improved. V and Mo can significantly improve the pitting-corrosion resistance of the alloys.

According to Equations (1) and (2), the corrosion rates of $TiZr_{0.5}NbCr_{0.5}$, $TiZr_{0.5}NbCr_{0.5}V$ and $TiZr_{0.5}NbCr_{0.5}Mo$ alloys are 3.55×10^{-3} mm/y, 1.44×10^{-4} mm/y and 3.69×10^{-4} mm/y, respectively, in in 0.5 M H_2SO_4 solution at 25 °C. It has been reported that CoCrFeNi alloy has the best resistance to corrosion in 0.5 M H_2SO_4 solution than other HEAs, and its corrosion rate is 0.12 mm/year [21]. However, compared with our alloys, its corrosion rate is much larger, indicating that the corrosion resistance of the three alloys in H_2SO_4 solution is better than CoCrFeNi alloy. Generally, the austenitic stainless steels are ternary iron-chromium-nickel alloys, and their structures are FCC type. The austenitic stainless steels normally have greater corrosion resistance than the ferrite stainless steels (BCC structure) [20–24]. Generally, there are always potential differences between different phases, and which facilitate to form micro-batteries. So, the resistance to corrosion of single DSS phase is better than that of multiphase alloys. Furthermore, single DSS FCC phase has a good resistance to corrosion than BCC phase or other multiphase structure, possibly due to its higher atomic packing density. Compared with traditional HEAs, especially CoCrFeNi alloy which has a FCC structure, this system of alloys that are composed of BCC DSS phase and Cr_2Zr phase has excellent corrosion resistance in the H_2SO_4 solution, possibly due to the passive elements and the high entropy phase structure in the alloys.

$TiZr_{0.5}NbCr_{0.5}V$ and $TiZr_{0.5}NbCr_{0.5}Mo$ alloys have lower corrosion rate than $TiZr_{0.5}NbCr_{0.5}$ alloy in H_2SO_4 solution, related with the strong ability to passive for Mo and V which can form protective passivation coatings on the surface of alloys in the acid solutions.

For $TiZr_{0.5}NbCr_{0.5}V$ alloy, corrosion initiates mainly on the boundaries of the BCC phase and Cr_2Zr Laves phase in NaCl solution at room temperature. The boundaries between different phases are the areas where are packed with crystal defects, impurities, alloying elements and where atomic arrangement is loose and disorder, which lead to be active in the boundaries and initiate corrosion. So, in the $TiZr_{0.5}NbCr_{0.5}V$ alloy, the boundaries of the two phases are the weak zones and preferential to initiate corrosion.

4. Experimental Section

4.1. Test Specimens for Electrochemical and Immersion Tests

Three refractory alloys were prepared by vacuum arc melting of the mixtures of high-purity metals with the purity better than 99 wt.% under a Ti-gettered high-purity argon atmosphere on a water-cooled Cu hearth. The alloys were remelted 4–5 times in order to improve homogeneity, the experimental details can consult Ref. [5]. For electrochemical test, the specimens were cut in $0.7 \times 0.7 \times 0.3$ cm^3, electrically connected to an isolated copper wire, and cold-mounted in epoxy with the outside surface of 0.7×0.7 cm^2 exposed. For immersion test, the samples cut in $0.7 \times 0.7 \times 0.3$ cm^3 were carefully mechanically polished with silicon carbide paper and dipped in 3.5% NaCl solution at 25 °C for 15 days.

4.2. Electrochemical Test

PP measurements were carried out in a typical three-electrode cell setup with the specimen as working electrode (WE), a saturated calomel electrode as reference electrode (RE), and a platinum plate as auxiliary electrode (AE), as shown in the Figure 6. The quasi-steady-state time for an open circuit voltage was 600 s. The specimen was scanned potentiodynamically at a rate of 1 mV/s from the initial potential of −1.0 V *versus* open circuit potential to the final potential of 1.5 V. The base solutions for the test were 3.5 wt.% NaCl and 0.5M H_2SO_4. The effect of temperature on polarization was examined at an interval of 15 °C in the temperature range of 25–55 °C in sodium chloride solution.

Figure 6. Schematic diagram of electrochemical experiment device.

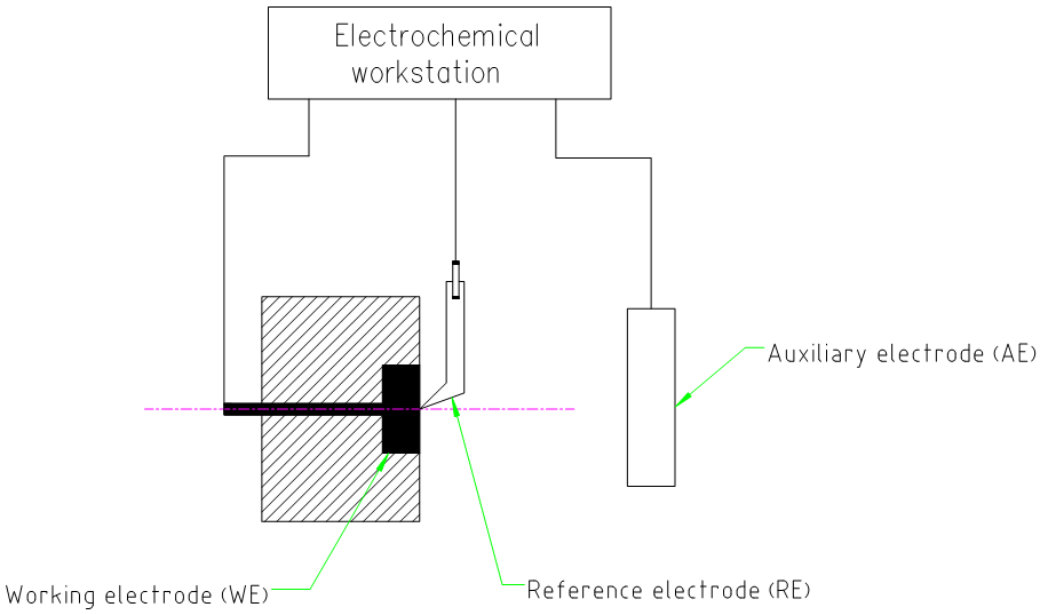

4.3. XRD and SEM Analysis

The crystal structure was identified by X-ray diffraction (XRD) using a PHILIPS APD-10 diffractometer with Cu Kα radiation and 2θ range of 20°–90°. The microstructure was analyzed with the use of a FEI Quanta250 scanning electron microscope (SEM, FEI, Hillsboro, OR, USA) equipped with energy dispersive spectrometry (EDS, FEI, Hillsboro, OR, USA).

5. Conclusions

A new series of $TiZr_{0.5}NbCr_{0.5}V_xMo_y$ refractory HEAs have been successfully prepared and their corrosion behaviors have been studied. All of $TiZr_{0.5}NbCr_{0.5}$, $TiZr_{0.5}NbCr_{0.5}V$ and $TiZr_{0.5}NbCr_{0.5}Mo$ alloys consist of BCC DSS phase and Cr_2Zr phase and exhibit obvious dendrite structures. BCC phase mainly concentrates on the dendrites and the inter-dendrites are ordered Cr_2Zr phase.

All alloys show excellent corrosion resistance in 3.5 wt.% NaCl and 0.5 M H_2SO_4 solutions. At room temperature, all alloys possess high corrosion potential, low corrosion current density, very wide passive region (>1400 mV) and positive pitting potential, which indicates they have good resistance to general corrosion and pitting.

The addition of V and Mo decreases the resistance to general corrosion and increases the pitting corrosion resistance for the series of alloys in NaCl solution slightly, while they greatly improve the corrosion resistance in H_2SO_4 solution. With temperature increasing, the corrosion rate of the alloys increases and the $TiZr_{0.5}NbCr_{0.5}V$ alloy is the least sensitive to temperature.

After immersion, no obvious corrosion regions are found on the surface of $TiZr_{0.5}NbCr_{0.5}$ alloy; localized corrosion initiates mainly on the boundaries between the BCC phase and Cr_2Zr phase.

In addition, obvious serration and electrochemical noise are observed on the PP curves, which may be related to the pitting process.

Acknowledgments

The authors acknowledge the financial support by National Natural Science Foundation of China (NSFC, granted No. 51210105006).

Author Contributions

All authors have made contributions to this paper. J.M Li, X. Yang and Y. Zhang conducted the experiments and wrote the paper; J.M. Li and X. Yang analyzed the results; J.M. Li and R.L. Zhu performed the corrosion and noise tests; X. Yang and Y. Zhang designed the experiments and revised the paper. All authors discussed the results and reviewed the manuscript.

Conflicts of Interest

The authors declare no conflict of interest.

References

1. Zhang, Y.; Lu, Z.P.; Ma, S.G.; Liaw, P.K.; Tang, Z.; Cheng, Y.Q.; Gao, M.C. Guidelines in predicting phase formation of high-entropy alloys. *MRS Commun.* **2014**, *4*, 57–62.
2. Middleburgh, S.C.; King, D.M.; Lumpkin, G.R.; Cortie, G.R.; Edwards, L. Segregation and migration of species in CrCoFeNi high entropy alloys. *J. Alloy. Compd.* **2014**, *599*, 179–182.
3. Zhang, C.; Zhang, F.; Chen, S.; Cao, W. Computational thermodynamics aided high entropy alloys design. *J. Miner. Metals Mater. Soc.* **2012**, *64*, 839–845.
4. Yeh, J.W.; Chen, S.K.; Lin, S.J.; Gan, J.Y.; Chin, T.S.; Shun, T.T.; Tsau, C.H.; Chang, S.Y. Nanostructured high-entropy alloys with multiple principal elements: Novel alloy design concepts and outcomes. *Adv. Eng. Mater.* **2004**, *6*, 299–303.
5. Hsu, Y.J.; Chiang, W.C.; Wu, J.K. Corrosion behavior of $FeCoNiCrCu_x$ high-entropy alloys in 3.5% sodium chloride solution. *Mater. Chem. Phys.* **2005**, *92*, 112–117.
6. Zhang, Y.; Zuo, T.T.; Tang, Z.; Gao, M.C.; Dahmen, K.A.; Liaw, P.K.; Lu, Z.P. Microstructure and properties of high entropy alloys. *Prog. Mater. Sci.* **2014**, *61*, 1–93.
7. Zhang, Y.; Zhou, Y.J.; Lin, J.P.; Chen, G.L.; Liaw, P.K. Solid-solution phase formation rules for multi-component alloys. *Adv. Eng. Mater.* **2008**, *10*, 534–538.
8. Zhang, Y.; Yang, X.; Liaw, P.K. Alloy design and properties optimization of high-entropy alloys. *J. Miner. Metals Mater. Soc.* **2012**, *64*, 830–838.

9. Shun, T.T.; Du, Y.C. Microstructure and tensile behaviors of FCC $Al_{0.3}CoCrFeNi$ high entropy alloy. *J. Alloy. Compd.* **2009**, *479*, 157–160.
10. Ma, S.G.; Zhang, S.F.; Qiao, J.W.; Wang, Z.H.; Gao, M.C.; Jiao, Z.M.; Yang, H.J.; Zhang, Y. Superior high tensile elongation of a single-crystal $CoCrFeNiAl_{0.3}$ high-entropy alloy by Bridgman solidification. *Intermetallics* **2014**, *54*, 104–109.
11. Zhang, Y.; Zuo, T.T.; Cheng, Y.Q.; Liaw, P.K. High-entropy alloys with high saturation magnetization, electrical resistivity, and malleability. *Sci. Rep.* **2013**, *3*, 1455.
12. Ren, B.; Zhao, R.F.; Liu, Z.X.; Guan, S.K.; Zhang, H.S. Microstructure and properties of $Al_{0.3}CrFe_{1.5}MnNi_{0.5}Ti_x$ and $Al_{0.3}CrFe_{1.5}MnNi_{0.5}Si_x$ high-entropy alloys. *Rare Metals* **2014**, *33*, 149–154.
13. Ren, B.; Liu, Z.X.; Cai, B.; Wang, M.X.; Shi, L. Aging behavior of a $CuCr_2Fe_2NiMn$ high-entropy alloy. *Mater. Des.* **2012**, *33*, 121–126.
14. Senkov, O.N.; Wilks, G.B.; Scott, J.M.; Miracle, D.B. Mechanical properties of $Nb_{25}Mo_{25}Ta_{25}W_{25}$ and $V_{20}Nb_{20}Mo_{20}Ta_{20}W_{20}$ refractory high entropy alloys. *Intermetallics* **2011**, *19*, 698–706.
15. Yang, X.; Zhang, Y.; Liaw, P.K. Microstructure and compressive properties of $NbTiVTaAl_x$ high entropy alloys. *Procedia Eng.* **2012**, *36*, 292–298.
16. Senkov, O.N.; Senkova, S.V.; Dimiduk, D.M.; Woodward, C.; Miracle, D.B. Oxidation behavior of a refractory $NbCrMo_{0.5}Ta_{0.5}TiZr$ alloy. *J. Mater. Sci.* **2012**, *47*, 6522–6534.
17. Stasko, R.; Adrian, H.; Adrian, A. Effect of nitrogen and vanadium on austenite grain growth kinetics of a low alloy steel. *Mater. Charact.* **2006**, *56*, 340–347.
18. Han, K.; Mottishaw, T.D.; Smith, G.D.W.; Edmonds, D.V.; Stacey, A.G. Effects of vanadium additions on microstructure and hardness of hypereutectoid pearlitic steels. *Mater. Sci. Eng. A* **1995**, *190*, 207–214.
19. Lin, C.M.; Tsai, H.L.; Bor, H.Y. Effect of aging treatment on microstructure and properties of high-entropy $Cu_{0.5}CoCrFeNi$ alloy. *Intermetallics* **2010**, *18*, 1244–1250.
20. Lin, C.M.; Tsai, H.L. Effect of annealing treatment on microstructure and properties of high-entropy $FeCoNiCrCu_{0.5}$ alloy. *Mater. Chem. Phys.* **2011**, *128*, 50–56.
21. Lee, C.P.; Chang, C.C.; Chen, Y.Y.; Yeh, J.W.; Shih, H.C. Effect of the aluminium content of $Al_xCrFe_{1.5}MnNi_{0.5}$ high-entropy alloys on the corrosion behaviour in aqueous environments. *Corros. Sci.* **2008**, *50*, 2053–2060.
22. Tao, L.C.; Chen, C.S.; Fan, K.H.; Huang, Y.T. Effect of the annealing treatment on the microstructure, microhardness and corrosion behaviour of $Al_{0.3}CrFe_{1.5}MnNi_{0.5}$ high-entropy alloys. *Adv. Mater. Res.* **2013**, *748*, 79–85.
23. Tang, Z.; Huang, L.; He, W.; Liaw, P.K. Alloying and processing effects on the aqueous corrosion behavior of high-entropy alloys. *Entropy* **2014**, *16*, 895–911.
24. Kao, Y.F.; Lee, T.D.; Chen, S.K.; Chang, Y.S. Electrochemical passive properties of $Al_xCoCrFeNi$ (x = 0, 0.25, 0.50, 1.00) alloys in sulfuric acids. *Corros. Sci.* **2010**, *52*, 1026–1034.